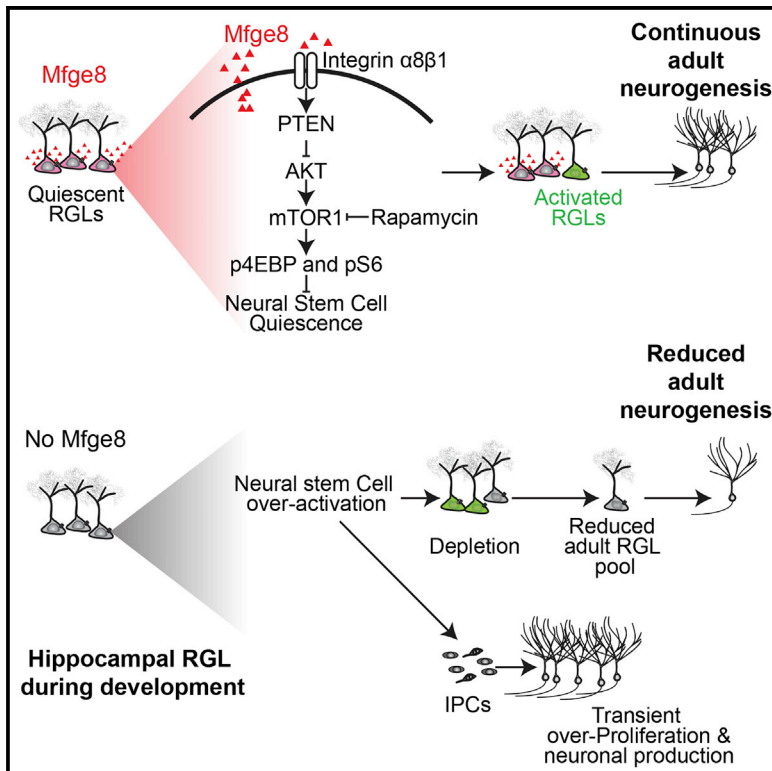# Cell Stem Cell

Autocrine Mfge8 Signaling Prevents Developmental Exhaustion of the Adult Neural Stem Cell Pool

Graphical Abstract

Authors

Yi Zhou, Allison M. Bond, Jamie E. Shade, ..., Kamran Atabai, Guo-li Ming, Hongjun Song

Correspondence

shongjun@pennmedicine.upenn.edu

In Brief

Zhou et al. identify Mfge8, traditionally known for its role in phagocytosis, as a neural-stem-cell-enriched niche factor that maintains the neural stem cell pool in the dentate gyrus during early postnatal development and in adulthood by promoting neural stem cell quiescence.

Highlights

- Mfge8 is enriched in quiescent neural stem cells

- *Mfge8* deletion depletes neural stem cells and decreases adult neurogenesis

- Mfge8 promotes early postnatal and adult neural stem cell quiescence

- Mfge8 regulates neural stem cell quiescence via mTOR1 signaling

CellPress

Autocrine Mfge8 Signaling Prevents Developmental Exhaustion of the Adult Neural Stem Cell Pool

Yi Zhou,[1,2] Allison M. Bond,[1] Jamie E. Shade,[3] Yunhua Zhu,[3] Chung-ha O. Davis,[4] Xinyuan Wang,[1] Yijing Su,[1] Ki-Jun Yoon,[1] Alexander T. Phan,[3] William J. Chen,[3,5] Justin H. Oh,[3] Nicholas Marsh-Armstrong,[4] Kamran Atabai,[6] Guo-li Ming,[1,7,8,9] and Hongjun Song[1,2,7,8,10,11,*]

[1]Department of Neuroscience, Mahoney Institute for Neurosciences, Perelman School of Medicine, University of Pennsylvania, Philadelphia, PA 19104, USA
[2]The Biochemistry, Cellular and Molecular Biology Graduate Program, Johns Hopkins University School of Medicine, Baltimore, MD 21205, USA
[3]Institute for Cellular Engineering, Johns Hopkins University School of Medicine, Baltimore, MD 21205, USA
[4]Hugo Moser Research Institute at Kennedy Krieger, Johns Hopkins University School of Medicine, Baltimore, MD 21205, USA
[5]Saint John's School, Houston, TX 77019, USA
[6]Cardiovascular Research Institute, Department of Medicine, Lung Biology Center, University of California, San Francisco, San Francisco, CA 94158, USA
[7]Department of Cell and Developmental Biology, University of Pennsylvania, Philadelphia, PA 19104, USA
[8]Institute for Regenerative Medicine, University of Pennsylvania, Philadelphia, PA 19104, USA
[9]Department of Psychiatry, University of Pennsylvania, Philadelphia, PA 19104, USA
[10]The Epigenetics Institute, Perelman School of Medicine, University of Pennsylvania, Philadelphia, PA 19104, USA
[11]Lead Contact
*Correspondence: shongjun@pennmedicine.upenn.edu
https://doi.org/10.1016/j.stem.2018.08.005

SUMMARY

Adult neurogenesis, arising from quiescent radial-glia-like neural stem cells (RGLs), occurs throughout life in the dentate gyrus. How neural stem cells are maintained throughout development to sustain adult mammalian neurogenesis is not well understood. Here, we show that milk fat globule-epidermal growth factor (EGF) 8 (Mfge8), a known phagocytosis factor, is highly enriched in quiescent RGLs in the dentate gyrus. *Mfge8*-null mice exhibit decreased adult dentate neurogenesis, and furthermore, adult RGL-specific deletion of *Mfge8* leads to RGL overactivation and depletion. Similarly, loss of *Mfge8* promotes RGL activation in the early postnatal dentate gyrus, resulting in a decreased number of label-retaining RGLs in adulthood. Mechanistically, loss of *Mfge8* elevates mTOR1 signaling in RGLs, inhibition of which by rapamycin returns RGLs to quiescence. Together, our study identifies a neural-stem-cell-enriched niche factor that maintains quiescence and prevents developmental exhaustion of neural stem cells to sustain continuous neurogenesis in the adult mammalian brain.

INTRODUCTION

Neurogenesis persists throughout life in the subgranular zone (SGZ) in the dentate gyrus of the hippocampus and the subventricular zone (SVZ) of the lateral ventricles (Gage, 2000). In the adult hippocampus, quiescent radial-glia-like neural stem cells (RGLs) continuously give rise to newborn dentate granule neurons and astrocytes (Ming and Song, 2011). Accumulative evidence has demonstrated critical roles of new neurons in the adult hippocampus in regulating neural plasticity as well as cognitive and affective behaviors, whereas deficits in adult hippocampal neurogenesis have been implicated in various brain disorders (Anacker and Hen, 2017; Christian et al., 2014). Therefore, understanding how the pool of adult neural stem cells is regulated during development and maintained in adulthood has implications for brain plasticity and regenerative medicine.

Both extrinsic environmental signals and intrinsic signaling pathways regulate the sequential process of neurogenesis in adult SGZ and SVZ, ranging from quiescent neural stem cell activation and fate specification to new neuron development and integration (Bond et al., 2015). Multiple lines of evidence suggest that RGL quiescence is a highly regulated state and is critical to maintain continuous neurogenesis in the adult brain. First, single-cell transcriptome analyses have revealed high expression levels of many signaling pathway receptors and intracellular mediators during quiescence, which become downregulated upon RGL activation (Llorens-Bobadilla et al., 2015; Shin et al., 2015). Second, dysregulation of cytoplasmic signaling pathways, such as FoxO (Paik et al., 2009; Renault et al., 2009) and phosphatase and tensin homolog (PTEN) (Bonaguidi et al., 2011), activates quiescent RGLs. Third, activation of quiescent RGLs can lead to their depletion in both adult SGZ and SVZ (Calzolari et al., 2015; Encinas et al., 2011; Mira et al., 2010; Seib et al., 2013). Understanding how adult neural stem cell quiescence is regulated remains an important cornerstone in the field and may have implications for understanding other somatic stem cells in various tissues. Among niche factors known to regulate adult RGL quiescence, almost all of them are paracrine factors, including neurotransmitters and peptides released from axon terminals (Berg et al., 2013), the Wnt inhibitor sFRP3 released
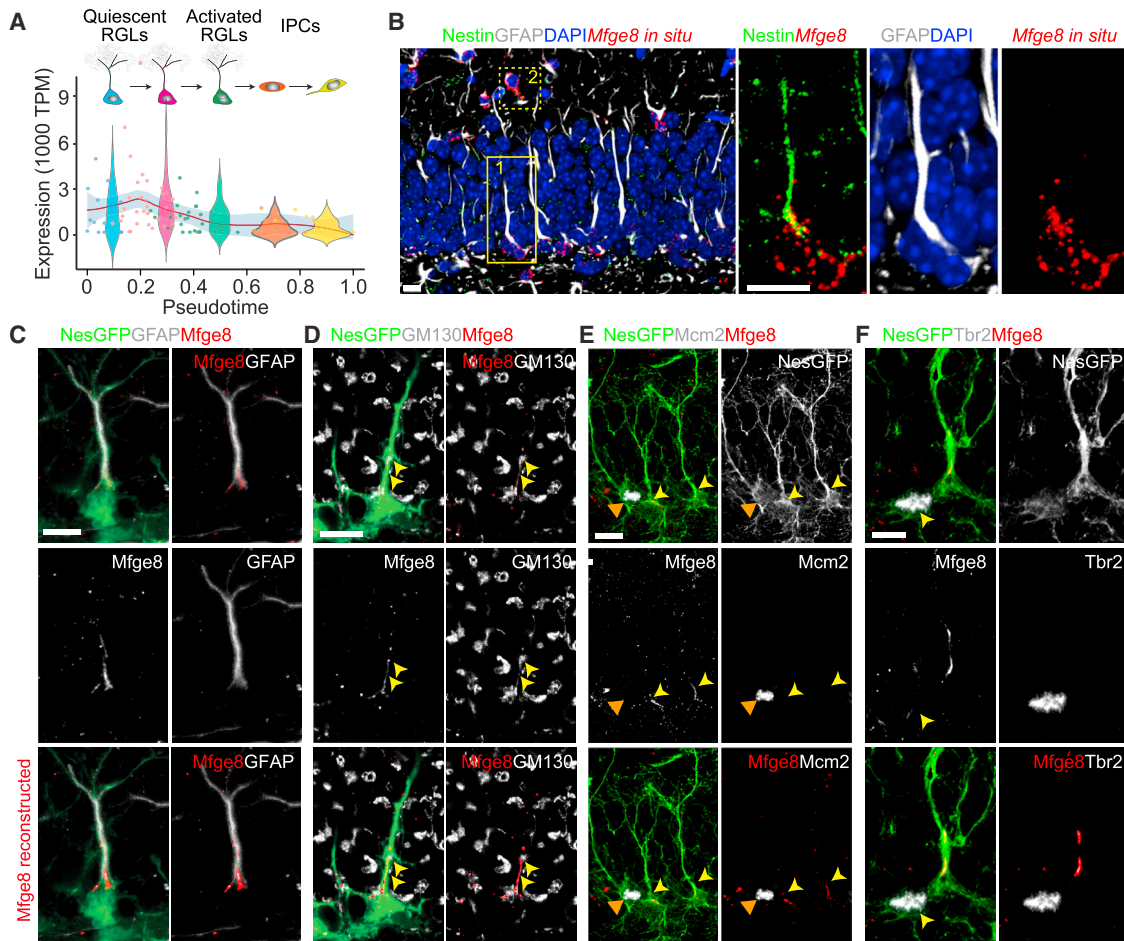
Figure 1. Mfge8 Is Enriched in Quiescent Adult Mouse Hippocampal Neural Stem Cells

(A) Enrichment of *Mfge8* mRNA in quiescent RGLs. Shown is an expression profile of *Mfge8* from single-cell RNA-seq analysis of Nestin-CFP marked neural progenitors in adult mouse dentate gyrus (Shin et al., 2015). Each data point represents the expression level of *Mfge8* of a single cell along a pseudotime trajectory from quiescent RGLs to activated RGLs to proliferating IPCs. Data points are fitted with local polynomial regression fitting (red line) with 95% confidence intervals (gray area). The superimposed Violin plots represent a summary of expression from different stages along the neurogenesis trajectory.

(B) Sample confocal images of *Mfge8* fluorescent *in situ* hybridization and Nestin and GFAP immunostaining in the adult mouse dentate gyrus. Note the presence of *Mfge8* mRNA in Nestin[+]GFAP[+] RGLs (an example in box 1 with solid line) and in Nestin[−]GFAP[+] astrocytes (an example in box 2 with dashed line). The region in box 1 is shown at a higher magnification (right panels). The scale bars represent 10 μm.

(C–F) Sample confocal images of immunostaining for Mfge8 and GFAP (C), Golgi marker GM130 (D; arrow points to Mfge8 and GM130 colocalization at the base of RGL radial fiber), proliferating cell marker Mcm2 (E; yellow arrowheads point to Mcm2^{−} RGLs and orange arrows point to a Mcm2^{+} RGL; see Video S1), and an intermediate progenitor cell (IPC) marker Tbr2 (F; arrow points to a Tbr2^{+} cell) in Nestin-GFP^{+} cells in adult mouse dentate gyrus. Bottom panel shows 3D volume-rendered Mfge8 immunostaining. The scale bars represent 10 μm. Note the presence of Mfge8 in GM130^{+} Golgi compartment in Mcm2^{−}Nestin-GFP[+]GFAP[+] quiescent RGLs, but not in Tbr2^{+} IPCs.

Also see Figure S1 and Video S1.

from mature granule cells (Jang et al., 2013), Notch ligand DLL1 from newborn neurons (Kawaguchi et al., 2013), and growth factors neurotrophin-3 (NT-3) and vascular endothelial growth factor (VEGF) released from endothelial cells (Delgado et al., 2014). Much less is known about whether RGL quiescence is also regulated by neural-stem-cell-derived factors.

Quiescence has also been suggested to be essential for establishing the adult neural stem cell pool during development. Neural stem cells that will populate the adult SVZ are set aside and remain quiescent during development (Fuentealba et al., 2015; Furutachi et al., 2015). Importantly, activation of these quiescent or slowly dividing populations during development,

by deletion of either the cyclin-dependent kinase inhibitor p57 (Furutachi et al., 2015) or VCAM1 (Hu et al., 2017), reduces the pool of adult SVZ neural stem cells. The niche mechanism that regulates the adult neural stem cell pool during development is completely unknown.

Our recent single-cell transcriptomic analysis has provided insight into the molecular signature of quiescent RGLs in the adult mouse dentate gyrus (Shin et al., 2015). We noted that the transcript of milk-fat globule-epidermal growth factor (EGF) factor 8 (Mfge8, also known as SED1 or lactadherin) is highly enriched during the quiescent state compared to the activated state of RGLs (Figure 1A). Mfge8 is traditionally known to play a critical

role in phagocytosis (Raymond et al., 2009). Phagocytes secrete Mfge8, which binds to "eat me" signals secreted by dying cells, such as exposed phosphatidylserine. Mfge8 then binds to integrin receptors $\alpha_v\beta_3$ or $\alpha_v\beta_5$ expressed on phagocytes to promote engulfment of apoptotic cells. In the nervous system, activated microglia or astrocytes during neuroinflammation or ischemic injury secrete Mfge8 and phagocytose dying cells and fragments (Fricker et al., 2012; Mills et al., 2015; Neher et al., 2013). Here, we investigated the physiological role and mechanism of Mfge8 in regulating early postnatal and adult neurogenesis.

RESULTS

Mfge8 Is Enriched in Quiescent RGLs in Adult Mouse Dentate Gyrus

Our recent single-cell RNA sequencing analysis suggested an enrichment of *Mfge8* mRNA in quiescent, but not active, neural progenitors in the adult mouse dentate gyrus (Figure 1A; Shin et al., 2015). To validate this result, we performed *in situ* hybridization in combination with immunohistology. Indeed, *Mfge8* mRNA was present in Nestin⁺GFAP⁺ RGLs and Nestin⁻GFAP⁺ astrocytes in the adult dentate gyrus (Figure 1B). Using Nestin-GFP transgenic mice (Encinas et al., 2006) to label adult RGLs and validated anti-Mfge8 antibodies (Figure S1A), we detected Mfge8 protein at the base of radial fibers in most Nestin-GFP⁺ GFAP⁺ RGLs (94.7% ± 3.3%; n = 3 mice) and in particular at the GM130⁺ Golgi apparatus (Figures 1C and 1D). Consistent with single-cell RNA sequencing results (Figure 1A), few proliferating Mcm2⁺ RGLs (16.2% ± 3.5%; n = 3; Figure 1E; Video S1) or Tbr2⁺ intermediate progenitor cells (IPCs) (6.1% ± 1.1%; n = 3; Figure 1F) expressed Mfge8 protein. Mfge8 protein was also present in s100β⁺ astrocytes (95.3% ± 4.5%; n = 3; Figure S1B) but was not detectable in NeuN⁺ mature granule cells, Iba1⁺ microglia, or Olig2⁺ oligodendrocyte precursors (n = 3; Figures S1C–S1E). Together, these results revealed highly enriched expression of Mfge8 in quiescent RGLs and astrocytes in the adult dentate gyrus.

Mfge8 Deletion Leads to Reduced Adult Hippocampal Neurogenesis

To explore the potential function of Mfge8 in the adult hippocampal neurogenesis, we first examined *Mfge8* homozygous germline knockout mice (KO) and their wild-type (WT) littermates (Hanayama et al., 2004). We injected bromodeoxyuridine (BrdU) into postnatal day 60 (P60) mice and collected tissue 2 hr later (Figure 2A). Quantification showed reduced densities of BrdU⁺Nestin⁺GFAP⁺ RGLs, BrdU⁺Tbr2⁺ IPCs, and BrdU⁺DCX⁺ neuroblasts (NBs) in KO mice compared to WT littermates (Figures 2B and 2C). We also examined proliferating cells independent of BrdU labeling with Mcm2 immunostaining and found similar results (Figures 2D and 2E). To examine the production of adult-born neurons, we injected P60 animals with BrdU five times at 12-hr intervals and collected tissue 30 days later (Figure 2F). We found a significant decrease in the density of BrdU⁺NeuN⁺ adult-born neurons in KO mice (Figures 2G and 2H). These results showed that Mfge8 is required to maintain a proper level of adult hippocampal neurogenesis.

Given that Mfge8 is expressed by both RGLs and astrocytes in the adult dentate gyrus, we next examined the specific contribu-

tion of Mfge8 from RGLs on adult neurogenesis. We generated the *Gli-CreER^T2::mT/mG^{f/+}::Mfge8^{f/f}* (cKO) model by crossing *Mfge8^{f/f}* conditional allele with the *Gli1-CreER^T2* driver, which specifically targets RGLs within the adult mouse dentate gyrus (Ahn and Joyner, 2005; Sun et al., 2015a), and with the *mT/mG^{f/+}* reporter (Muzumdar et al., 2007). We injected P60 mice with multiple doses of tamoxifen for analysis 30 days later (Figure 2I). Quantification showed a significant decrease in the density of GFP⁺ RGLs in the adult dentate gyrus of cKO mice (Figures 2J and 2K). In parallel, we observed a decrease in the number of GFP⁺ neuronal progeny, but an increase in GFP⁺ astrocytes (Figure 2K). These results suggest that adult RGL-derived Mfge8 is required to maintain proper RGL numbers and adult neurogenesis levels and to prevent RGL depletion via differentiation into astrocytes.

Mfge8 Promotes RGL Quiescence in the Adult and Early Postnatal Dentate Gyrus

Activation of quiescent RGLs can lead to their depletion via differentiation into astrocytes in the adult dentate gyrus (Bonaguidi et al., 2011; Encinas et al., 2011). To determine whether RGLs were overactivated, we performed short-term fate mapping upon adult RGL-specific *Mfge8* deletion. We injected tamoxifen into P60 cKO mice and analyzed 3 days later (Figure 3A). Quantification of Mcm2⁺ GFP⁺ RGLs among all GFP⁺ RGLs showed a significant increase in cKO mice (Figures 3B and 3C). Thus, Mfge8 functions to promote adult dentate RGL quiescence.

This result of increased RGL activation in the adult RGL-specific cKO model is in contrast to the decreased density of dividing RGLs in the adult dentate gyrus of the germline KO model (Figures 2B–2E). One possibility is that the loss of Mfge8 leads to premature activation and depletion of RGLs during early postnatal development, resulting in a decreased total number of RGLs, which in turn leads to a reduced number of proliferating RGLs and a decreased level of adult dentate neurogenesis (Figure S2A).

We directly tested this hypothesis by analyzing early postnatal dentate neurogenesis. Immunohistological analyses showed that Mfge8 was expressed in most Mcm2⁻ quiescent RGLs from P3 to adult (Figure S2B). We pulsed WT and KO mice at P15 with BrdU and analyzed 2 hr later (Figure 3D). Quantification showed significantly increased densities of BrdU⁺Nestin⁺GFAP⁺ RGLs, BrdU⁺Tbr2⁺ IPCs, and BrdU⁺DCX⁺ NBs in KO mice (Figures 3E and 3F). Analysis of proliferating cells based on Mcm2 expression showed similar results (Figures 3G and 3H). To examine the long-term consequences, we pulsed animals with multiple BrdU injections at P15 for analysis 30 days later (Figure 3I). Consistent with increased RGL activation and increased numbers of IPCs and NBs at P15, we found an increased density of BrdU⁺NeuN⁺ mature neurons in KO mice (Figures 3J and 3K). Importantly, the density of BrdU⁺Nestin⁺GFAP⁺ labeling-retaining RGLs was significantly reduced in KO mice (Figures 3L and 3M), indicating a reduced pool of adult RGLs in the absence of Mfge8. Similarly, conditional deletion of *Mfge8* with *Gli-CreER^T2* at P15 led to a reduced number of GFP⁺ RGLs examined 30 days later (Figures 3N and 3O). At the population level, KO mice exhibited a slight increase of Nestin⁺GFAP⁺ RGLs and significant increase of Tbr2⁺ IPCs and BrdU⁺ or Mcm2⁺ proliferating progenitors at P15, in contrast to significant decreases in these cell populations at P60 (Figures S2D–S2F).
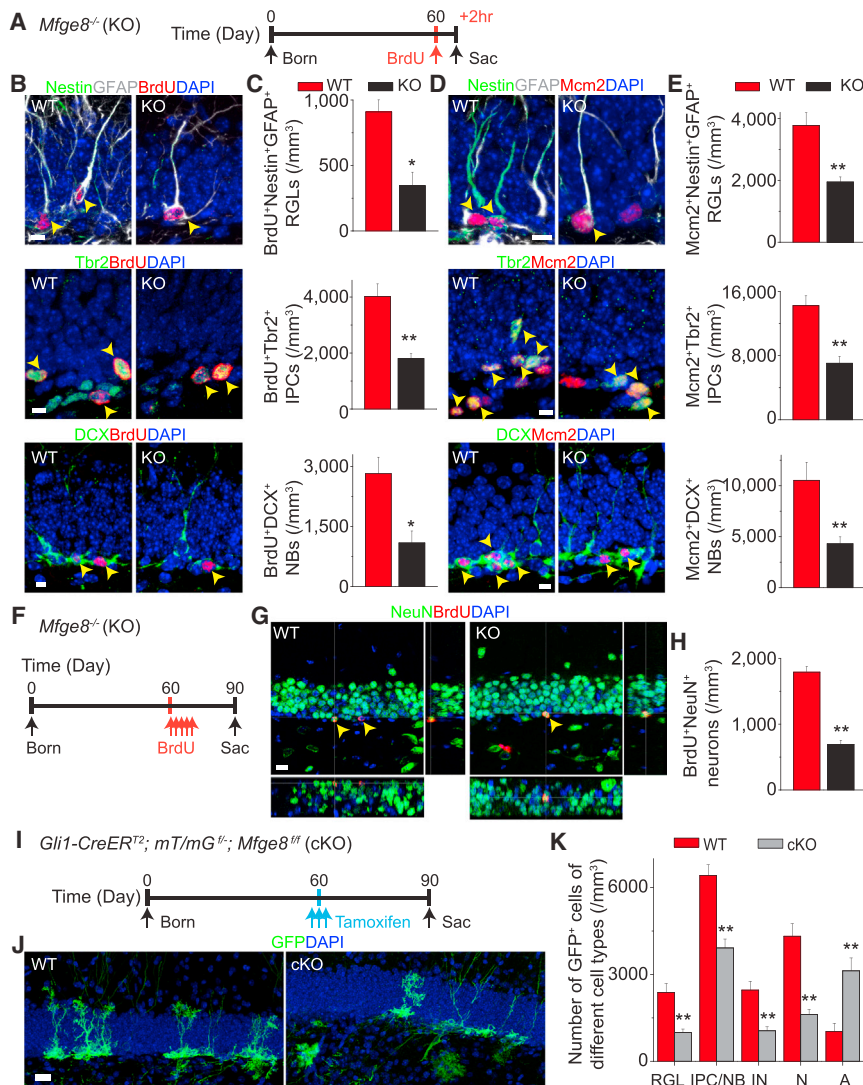
Figure 2. *Mfge8* Deletion Leads to Decreased Adult Hippocampal Neurogenesis

(A–E) Reduced densities of proliferating RGLs, IPCs, and neuroblasts (NBs) in the dentate gyrus of P60 *Mfge8* KO mice. Shown in (A) is a schematic diagram of experimental design of a 2-hr BrdU pulse chase in P60 mice. Also shown are sample confocal images (B and D) and quantification (C and E) of Nestin$^+$GFAP$^+$ RGLs, Tbr2$^+$ IPCs, and DCX$^+$ NBs that were BrdU$^+$ or Mcm2$^+$. Arrows point to BrdU$^+$ or Mcm2$^+$ marker$^+$ cells. The scale bars represent 10 μm. Values represent mean ± SEM (n = 5 for C and E; **p < 0.001; *p < 0.01; unpaired Student's t test).

(F–H) Reduced generation of adult-born neurons in the dentate gyrus of *Mfge8* KO mice. Shown in (F) is a schematic diagram of the experimental design of 30-day BrdU pulse chase in P60 mice. Also shown are sample confocal images (G) and quantification (H) of adult-born BrdU$^+$NeuN$^+$ dentate granule neurons. The scale bar represents 10 μm. Values represent mean ± SEM (n = 5; **p < 0.001; unpaired Student's t test).

(I–K) Reduced RGL maintenance and neurogenesis but increased astrocyte production upon conditional *Mfge8* deletion specifically in adult RGLs. Shown in (I) is a schematic diagram of experimental design of 30-day chase post-tamoxifen induction of P60 mice. Also shown are sample confocal images (J) and quantification of composition of GFP$^+$ cells in the dentate gyrus 1 month after induction (K). The scale bar represents 10 μm. Values represent mean ± SEM (n = 5; **p < 0.001; unpaired Student's t test). A, astrocyte; IN, immature neuron; N, mature neuron.

Together, these results support the model that RGL-derived Mfge8 promotes RGL quiescence and maintenance in early postnatal stages to sustain a proper level of dentate neurogenesis into adulthood.

Mfge8 Promotes RGL Quiescence via Suppression of mTOR1 Pathway

We next examined how Mfge8 maintains RGL quiescence. Integrin $\alpha_v\beta_{3/5}$ is the best known Mfge8 receptor for phagocytosis (Nagata et al., 2010; Figure S3A). However, immunohistological analysis showed that integrin β_5 does not appear to be expressed by RGLs but instead is co-localized almost exclusively with Iba1$^+$ microglia in the adult dentate gyrus (Figures S3B and S3D). This result raised the question of whether Mfge8-dependent regulation of RGLs involves microglia. Quantitative analyses showed no detectable differences in the densities of Iba1$^+$Itgb5$^+$ microglia or Iba1$^+$CD68$^+$-activated microglia between the WT and KO adult dentate gyrus (Figures S3D and S3E). Thus, microglia activity does not appear to be affected by the loss of Mfge8 in the dentate gyrus.

Integrin receptor $\alpha_8\beta_1$ was recently identified as a non-canonical Mfge8 receptor in regulating gastrointestinal motility (Figure S3A; Khalifeh-Soltani et al., 2016). Integrin β_1 is known to be expressed in neural progenitor cells in the adult SVZ and SGZ (Brooker et al., 2016; Shen et al., 2008). Indeed, immunohistological analysis showed expression of both integrin α_8 and β_1 by Nestin-GFP$^+$ RGLs in the P15 and P60 dentate gyrus (Figures 4A and S3C). We next used an *in vitro* adult neural progenitor cell culture model (Ma et al., 2008) to examine the role of integrin β_1 in regulating neural stem cell proliferation. We first confirmed that Mfge8 protein is released into the culture medium by adult neural progenitors (Figure 4B). Addition of recombinant Mfge8 protein reduced proliferation of adult neural progenitors (Figures 4C–4E and S3F). Importantly, addition of functional blocking antibodies for integrin β_1 (Goh et al., 2008), but not integrin α_v, abolished the effect of Mfge8 on suppression of adult neural progenitor proliferation (Figures 4C–4E).

Previous studies in the gastrointestinal system have shown that Mfge8 can either upregulate (Khalifeh-Soltani et al., 2014) or downregulate (Khalifeh-Soltani et al., 2016) the intracellular PTEN-phosphatidylinositol 3-kinase (PI3K)-Akt pathway by binding to integrin receptors $\alpha_v\beta_{3/5}$ or $\alpha_8\beta_1$, respectively (Figure S3A). One major target of the PTEN-Akt pathway is mTOR1,
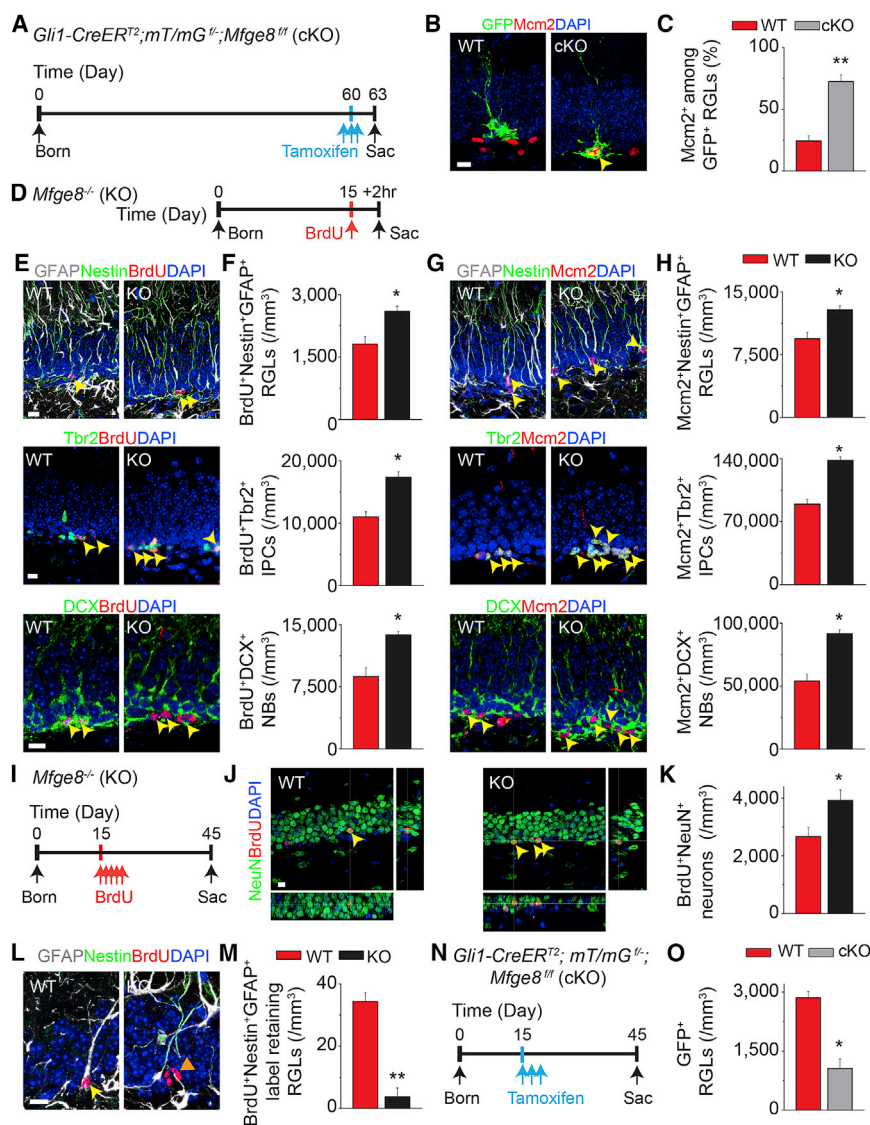
Figure 3. Mfge8 Suppresses RGL Activation and Prevents Developmental Exhaustion of RGLs in the Dentate Gyrus

(A–C) Conditional deletion of *Mfge8* in adult RGLs leads to their activation. Shown in (A) is a schematic diagram of experimental design. Shown in (B) are sample confocal images. Arrowhead points to a Mcm2⁺GFP⁺ RGL. The scale bar represents 10 μm. Shown in (C) are quantifications. Values represent mean ± SEM (n = 4; **p < 0.001; unpaired Student's t test).

(D–H) Lack of *Mfge8* leads to an increased number of proliferating RGLs, IPCs, and NBs in P15 dentate gyrus. Shown in (D) is a schematic diagram of experimental design of a 2-hr BrdU pulse chase in P15 mice. Also shown are sample confocal images (E and G) and quantifications (F and H) of Nestin⁺GFAP⁺ RGLs, Tbr2⁺ IPCs, and DCX⁺ NBs that were BrdU⁺ or Mcm2⁺. The scale bars represent 10 μm. Arrowheads point to BrdU⁺ or Mcm2⁺ and marker⁺ cells. Values represent mean ± SEM (n = 4 for E and H; *p < 0.01; unpaired Student's t test).

(I–M) Loss of Mfge8 leads to increased neurogenesis in early postnatal dentate gyrus but reduced number of RGLs in the adult dentate gyrus. Shown in (I) is a schematic diagram of the experimental design of 30-day BrdU pulse chase in P15 mice. Also shown are sample confocal images (J and L) and quantification of BrdU⁺⁻ NeuN⁺ early postnatally born granule neurons (K) and BrdU⁺Nestin⁺GFAP⁺ label-retaining RGLs (M) 30 days after BrdU injection. Yellow arrows point to BrdU⁺NeuN⁺ neurons (J) or BrdU⁺Nestin⁺⁻ GFAP⁺ label-retaining RGL (L). An orange arrowhead points to a BrdU⁺Nestin⁻GFAP⁻ cell (L). The scale bars represent 10 μm. Values represent mean ± SEM (n = 5 for K and M; *p < 0.01; **p < 0.001; unpaired Student's t test).

(N and O) Conditional deletion of *Mfge8* in RGLs at P15 leads to a decreased number of RGLs at P45. Shown are a schematic diagram of experimental design (N) and quantification (O). Values represent mean ± SEM (n = 4; *p < 0.01; unpaired Student's t test).

Also see Figure S2.

which is known to be required for neural stem cell proliferation (Ka et al., 2014; Sato et al., 2010). We found that, in cultured adult neural progenitors, exogenous Mfge8 reduced levels of phosphorylated AKT (pAKT), phosphorylated 4EBP1 protein (p4EBP1), and phosphorylated S6 protein (pS6) (Figures 4F and 4G). Such effects were blocked by anti-integrin β₁ antibodies, but not by anti-αᵥ antibodies (Figures 4F and 4G). Immunohistological analyses also showed a significant increase in densities of p4EBP1⁺ and pS6⁺ GFAP⁺ RGLs in KO mice at P15 (Figures 4G and 4H) and in the cKO model in the adult dentate gyrus (Figures S3G and S3H). These results suggest that Mfge8 serves as a suppressor of mTOR1 activation in neural stem cells (Figure S4A).

To assess the functional role of the mTOR1 pathway in Mfge8-dependent regulation of RGL quiescence, we pharmacologically inhibited mTOR1 activation with rapamycin injections at P11 and P13 and performed analysis at P15 (Figure 4I). Immunohistological analysis confirmed the effectiveness of rapamycin treatment

on reducing p4EBP1 and pS6 expression (Figures S4B and S4C). Quantification of Mcm2⁺ Nestin⁺GFAP⁺ RGLs in the dentate gyrus showed that, although rapamycin had no effect on WT animals, it completely abolished elevated RGL activation in *Mfge8* KO mice (Figure 4J). Similarly, rapamycin treatment abolished *Mfge8*-deletion-induced adult RGL activation in the cKO model (Figures S4D–S4F).

DISCUSSION

How the neural stem cell pool is maintained throughout early development to ensure a sufficient number of adult neural stem cells to support life-long neurogenesis is not well understood (Berg et al., 2018). Here, we identified Mfge8 as a stem-cell-enriched niche factor that maintains the adult neural stem cell pool during early postnatal development and in adulthood by promoting RGL quiescence (Figure S2A). In addition to a large number of previously identified paracrine factors released by
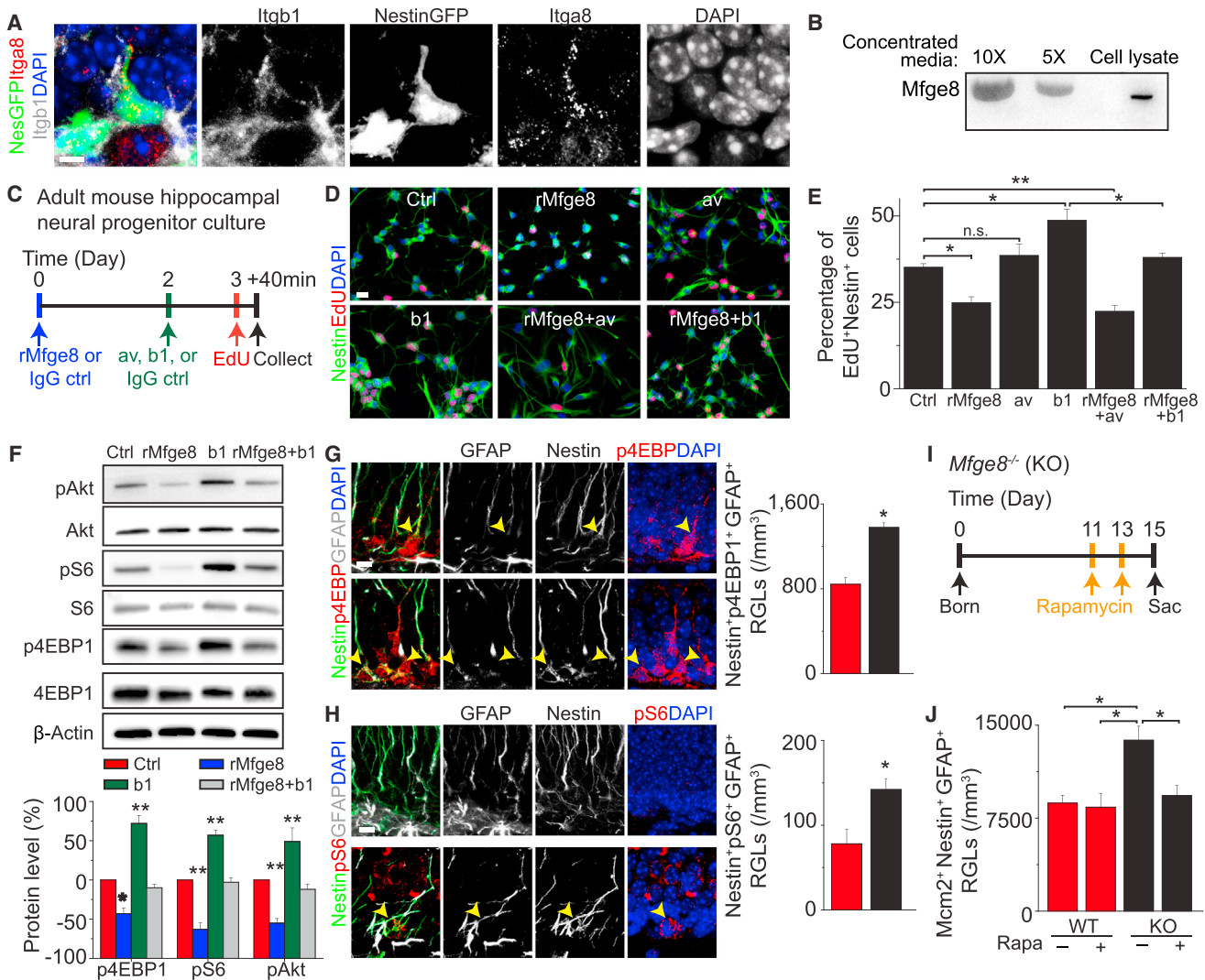
Figure 4. Mfge8 Promotes RGL Quiescence by Suppressing mTOR1 Signaling

(A) Sample confocal images of immunostaining for Mfge8, integrin receptor $\alpha_8\beta_1$ in Nestin-GFP$^+$ RGLs in the P15 dentate gyrus. The scale bar represents 10 μm.

(B) Release of Mfge8 protein into the culture medium of adult neural progenitors. Shown is a sample western blot of concentrated culture medium (10× and 5×) and whole-cell lysate.

(C–E) Mfge8 suppresses proliferation of adult neural progenitors. Shown are a schematic diagram of the experimental design (C), sample confocal images (D; scale bar: 20 μm), and quantifications (E) of adult mouse dentate-gyrus-derived neural progenitors cultured in the presence or absence of rMfge8 (0.5 μg/mL), anti-α_v integrin antibodies (av; 0.625 μg/mL), or anti-β_1 integrin antibodies (b1; 0.625 μg/mL). Values represent mean ± SEM (n = 4; **p < 0.001; *p < 0.01; n.s.: not significant; one-way ANOVA).

(F) Mfge8 suppresses mTOR1 signaling in adult neural progenitors. Adult neural progenitors were similarly treated as in (C) and then subject to western blot analysis. Shown are sample western blot images (top panels) and quantifications (bottom panel). Values represent mean ± SEM (n = 4; **p < 0.001; *p < 0.01; one-way ANOVA).

(G and H) Increased mTOR1 signaling in RGLs in *Mfge8* KO mice. Shown are sample confocal images and quantifications of numbers of p4EBP1$^+$ (G) and pS6$^+$ (H) Nestin$^+$GFAP$^+$ RGLs in P15 mice. Arrowheads point to p4EBP1$^+$ or pS6$^+$ Nestin$^+$GFAP$^+$ RGLs. The scale bars represent 10 μm. Values represent mean ± SEM (n = 4; *p < 0.01; unpaired Student's t test).

(I and J) Rapamycin treatment rescues RGL overactivation in the P15 dentate gyrus of *Mfge8* KO mice. Shown in (I) is a schematic diagram of the experimental design. Rapamycin (20 mg/kg body weight) or vehicle was intraperitoneally (i.p.) injected. Shown in (J) is the quantification of BrdU$^+$Nestin$^+$GFAP$^+$ RGLs. Values represent mean ± SEM (n = 4; *p < 0.01; one-way ANOVA).

Also see Figures S3 and S4.

other niche cell types, our finding illustrates the complexity of neurogenesis regulation that is also modulated by a stem-cell-derived factor *in vivo*. Although Mfge8 is best known to mediate phagocytosis, here, we identified a non-canonical role of Mfge8

signaling in maintaining neural stem cell quiescence by suppressing mTOR1 activation (Figure S4A). Interestingly, recent transcriptome analyses have also found enrichment of Mfge8 in different stem cell populations, such as neural stem cells in

the embryonic cortex (Pollen et al., 2015; Yuzwa et al., 2017; Zeisel et al., 2015), developing and adult dentate gyrus (Hochgerner et al., 2018), adult SVZ (Dulken et al., 2017), hair follicle stem cells (Lay et al., 2016), and pluripotent stem cells (Yan et al., 2013). These findings raise the possibility that Mfge8 may play a general role as an autocrine signal for various types of stem cells.

Mfge8 is traditionally known to be involved in phagocytosis by phagocytes and microglia (Raymond et al., 2009). In the adult dentate gyrus, however, Mfge8 is selectively expressed by quiescent RGLs and astrocytes, but not by RGL progeny or microglia. Through adult RGL-specific deletion, we provide evidence that the RGL population regulates its own quiescence and maintenance via Mfge8. One advantage of autocrine regulation is the spatial proximity of signals for fine tuning of stem cell behavior. Given diffusion limits of secreted molecules in the adult mammalian brain, especially when their receptors are in proximity for efficient trapping, effects could be spatially restricted. Astrocytes are known to modulate adult dentate neurogenesis via secreted factors (Lie et al., 2005; Ma et al., 2005; Song et al., 2002), and it will be interesting to examine whether astrocyte-derived Mfge8 also regulates RGL quiescence when genetic tools become available in the future. Because astrocytes are born during later postnatal stages (Figure S2C), it is likely that RGL-derived Mfge8 plays a more dominant role in regulating RGL quiescence during early postnatal development. Our study also identifies the signaling mechanism whereby Mfge8 promotes RGL quiescence (Figure S4A). Our results are consistent with previous findings that loss of integrin β_1 depletes RGLs, promotes astrocyte differentiation, and reduces neurogenesis in the adult dentate gyrus (Brooker et al., 2016). Notably, genetic deletion of *Ilk* (integrin-linked kinase) or *Pten* also leads to quiescent RGL activation in the adult dentate gyrus (Bonaguidi et al., 2011; Porcheri et al., 2014). Together, these findings identify the PTEN-Akt-mTOR1 pathway as a hub that integrates stem-cell-activation signals to regulate RGL quiescence and maintenance.

How the adult neural stem cell pool is regulated during development is not well understood. Recent studies have suggested a critical role for quiescence in preserving the somatic stem cell pool during development. For example, the adult muscle stem cell pool is established during puberty by sex-hormone-dependent regulation of Notch signaling that converts cycling juvenile stem cells to a quiescent stem cell population (Kim et al., 2016). For epidermal stem cells, NFATc1 (Horsley et al., 2008) and Lrig1 (Jensen et al., 2009) play a critical role in governing the quiescence of a reservoir of stem cells throughout hair follicle morphogenesis, which is retained during adulthood. In the CNS, activation of the reserve neural stem cells during development by deletion of p57 or VCAM1 reduces their numbers in the adult SVZ (Furutachi et al., 2015; Hu et al., 2017). Similarly, deletion of *FoxOs* leads to increased early postnatal hippocampal neurogenesis but a reduced number of RGLs and decreased neurogenesis in the adult hippocampus (Paik et al., 2009; Renault et al., 2009), a phenotype very similar to *Mfge8* KO mice. Our study identifies a stem-cell-enriched niche mechanism that maintains neural stem cell quiescence to sustain neurogenesis in the adult hippocampus. Our finding also highlights the complexity of prospective regulatory mechanisms to maintain a viable stem cell pool over the lifespan, involving both paracrine and autocrine signaling from a stem-cell-derived factor.

STAR★METHODS

Detailed methods are provided in the online version of this paper and include the following:

- KEY RESOURCES TABLE
- CONTACT FOR REAGENT AND RESOURCE SHARING
- EXPERIMENTAL MODEL AND SUBJECT DETAILS
  - Animals
- METHOD DETAILS
  - BrdU administration
  - Tamoxifen administration
  - Rapamycin administration
  - Tissue processing, immunostaining, and confocal imaging
  - *In situ* hybridization
  - Adult neural progenitor culture and analyses
  - Image processing and data analyses
- QUANTIFICATION AND STATISTICAL ANALYSIS

REFERENCES

Ahn, S., and Joyner, A.L. (2005). In vivo analysis of quiescent adult neural stem cells responding to Sonic hedgehog. Nature *437*, 894–897.

Anacker, C., and Hen, R. (2017). Adult hippocampal neurogenesis and cognitive flexibility - linking memory and mood. Nat. Rev. Neurosci. *18*, 335–346.

Berg, D.A., Belnoue, L., Song, H., and Simon, A. (2013). Neurotransmitter-mediated control of neurogenesis in the adult vertebrate brain. Development *140*, 2548–2561.

Berg, D.A., Bond, A.M., Ming, G.L., and Song, H. (2018). Radial glial cells in the adult dentate gyrus: what are they and where do they come from? F1000Res. *7*, 277.

Bonaguidi, M.A., Wheeler, M.A., Shapiro, J.S., Stadel, R.P., Sun, G.J., Ming, G.L., and Song, H. (2011). In vivo clonal analysis reveals self-renewing and multipotent adult neural stem cell characteristics. Cell *145*, 1142–1155.

Bond, A.M., Ming, G.L., and Song, H. (2015). Adult mammalian neural stem cells and neurogenesis: Five decades later. Cell Stem Cell *17*, 385–395.

Brooker, S.M., Bond, A.M., Peng, C.Y., and Kessler, J.A. (2016). β1-integrin restricts astrocytic differentiation of adult hippocampal neural stem cells. Glia *64*, 1235–1251.

Calzolari, F., Michel, J., Baumgart, E.V., Theis, F., Götz, M., and Ninkovic, J. (2015). Fast clonal expansion and limited neural stem cell self-renewal in the adult subependymal zone. Nat. Neurosci. *18*, 490–492.

Christian, K.M., Song, H., and Ming, G.L. (2014). Functions and dysfunctions of adult hippocampal neurogenesis. Annu. Rev. Neurosci. *37*, 243–262.

Delgado, A.C., Ferrón, S.R., Vicente, D., Porlan, E., Perez-Villalba, A., Trujillo, C.M., D'Ocón, P., and Fariñas, I. (2014). Endothelial NT-3 delivered by vasculature and CSF promotes quiescence of subependymal neural stem cells through nitric oxide induction. Neuron *83*, 572–585.

Dulken, B.W., Leeman, D.S., Boutet, S.C., Hebestreit, K., and Brunet, A. (2017). Single-cell transcriptomic analysis defines heterogeneity and transcriptional dynamics in the adult neural stem cell lineage. Cell Rep. *18*, 777–790.

Encinas, J.M., Vaahtokari, A., and Enikolopov, G. (2006). Fluoxetine targets early progenitor cells in the adult brain. Proc. Natl. Acad. Sci. USA *103*, 8233–8238.

Encinas, J.M., Michurina, T.V., Peunova, N., Park, J.H., Tordo, J., Peterson, D.A., Fishell, G., Koulakov, A., and Enikolopov, G. (2011). Division-coupled astrocytic differentiation and age-related depletion of neural stem cells in the adult hippocampus. Cell Stem Cell *8*, 566–579.

Fricker, M., Neher, J.J., Zhao, J.W., Théry, C., Tolkovsky, A.M., and Brown, G.C. (2012). MFG-E8 mediates primary phagocytosis of viable neurons during neuroinflammation. J. Neurosci. *32*, 2657–2666.

Fuentealba, L.C., Rompani, S.B., Parraguez, J.I., Obernier, K., Romero, R., Cepko, C.L., and Alvarez-Buylla, A. (2015). Embryonic origin of postnatal neural stem cells. Cell *161*, 1644–1655.

Furutachi, S., Miya, H., Watanabe, T., Kawai, H., Yamasaki, N., Harada, Y., Imayoshi, I., Nelson, M., Nakayama, K.I., Hirabayashi, Y., and Gotoh, Y. (2015). Slowly dividing neural progenitors are an embryonic origin of adult neural stem cells. Nat. Neurosci. *18*, 657–665.

Gage, F.H. (2000). Mammalian neural stem cells. Science *287*, 1433–1438.

Goh, E.L., Young, J.K., Kuwako, K., Tessier-Lavigne, M., He, Z., Griffin, J.W., and Ming, G.L. (2008). beta1-integrin mediates myelin-associated glycoprotein signaling in neuronal growth cones. Mol. Brain *1*, 10.

Hanayama, R., Tanaka, M., Miyasaka, K., Aozasa, K., Koike, M., Uchiyama, Y., and Nagata, S. (2004). Autoimmune disease and impaired uptake of apoptotic cells in MFG-E8-deficient mice. Science *304*, 1147–1150.

Hochgerner, H., Zeisel, A., Lönnerberg, P., and Linnarsson, S. (2018). Conserved properties of dentate gyrus neurogenesis across postnatal development revealed by single-cell RNA sequencing. Nat. Neurosci. *21*, 290–299.

Horsley, V., Aliprantis, A.O., Polak, L., Glimcher, L.H., and Fuchs, E. (2008). NFATc1 balances quiescence and proliferation of skin stem cells. Cell *132*, 299–310.

Hu, X.L., Chen, G., Zhang, S., Zheng, J., Wu, J., Bai, Q.R., Wang, Y., Li, J., Wang, H., Feng, H., et al. (2017). Persistent expression of VCAM1 in radial glial cells is required for the embryonic origin of postnatal neural stem cells. Neuron *95*, 309–325.e6.

Jang, M.H., Bonaguidi, M.A., Kitabatake, Y., Sun, J., Song, J., Kang, E., Jun, H., Zhong, C., Su, Y., Guo, J.U., et al. (2013). Secreted frizzled-related protein 3 regulates activity-dependent adult hippocampal neurogenesis. Cell Stem Cell *12*, 215–223.

Jensen, K.B., Collins, C.A., Nascimento, E., Tan, D.W., Frye, M., Itami, S., and Watt, F.M. (2009). Lrig1 expression defines a distinct multipotent stem cell population in mammalian epidermis. Cell Stem Cell *4*, 427–439.

Ka, M., Condorelli, G., Woodgett, J.R., and Kim, W.Y. (2014). mTOR regulates brain morphogenesis by mediating GSK3 signaling. Development *141*, 4076–4086.

Kawaguchi, D., Furutachi, S., Kawai, H., Hozumi, K., and Gotoh, Y. (2013). Dll1 maintains quiescence of adult neural stem cells and segregates asymmetrically during mitosis. Nat. Commun. *4*, 1880.

Khalifeh-Soltani, A., McKleroy, W., Sakuma, S., Cheung, Y.Y., Tharp, K., Qiu, Y., Turner, S.M., Chawla, A., Stahl, A., and Atabai, K. (2014). Mfge8 promotes obesity by mediating the uptake of dietary fats and serum fatty acids. Nat. Med. *20*, 175–183.

Khalifeh-Soltani, A., Ha, A., Podolsky, M.J., McCarthy, D.A., McKleroy, W., Azary, S., Sakuma, S., Tharp, K.M., Wu, N., Yokosaki, Y., et al. (2016). α8β1 integrin regulates nutrient absorption through an Mfge8-PTEN dependent mechanism. eLife *5*, e13063.

Kim, J.Y., Duan, X., Liu, C.Y., Jang, M.H., Guo, J.U., Pow-anpongkul, N., Kang, E., Song, H., and Ming, G.L. (2009). DISC1 regulates new neuron development in the adult brain via modulation of AKT-mTOR signaling through KIAA1212. Neuron *63*, 761–773.

Kim, J.H., Han, G.C., Seo, J.Y., Park, I., Park, W., Jeong, H.W., Lee, S.H., Bae, S.H., Seong, J., Yum, M.K., et al. (2016). Sex hormones establish a reserve pool of adult muscle stem cells. Nat. Cell Biol. *18*, 930–940.

Lay, K., Kume, T., and Fuchs, E. (2016). FOXC1 maintains the hair follicle stem cell niche and governs stem cell quiescence to preserve long-term tissue-regenerating potential. Proc. Natl. Acad. Sci. USA *113*, E1506–E1515.

Lie, D.C., Colamarino, S.A., Song, H.J., Désiré, L., Mira, H., Consiglio, A., Lein, E.S., Jessberger, S., Lansford, H., Dearie, A.R., and Gage, F.H. (2005). Wnt signalling regulates adult hippocampal neurogenesis. Nature *437*, 1370–1375.

Llorens-Bobadilla, E., Zhao, S., Baser, A., Saiz-Castro, G., Zwadlo, K., and Martin-Villalba, A. (2015). Single-cell transcriptomics reveals a population of dormant neural stem cells that become activated upon brain injury. Cell Stem Cell *17*, 329–340.

Ma, D.K., Ming, G.L., and Song, H. (2005). Glial influences on neural stem cell development: cellular niches for adult neurogenesis. Curr. Opin. Neurobiol. *15*, 514–520.

Ma, D.K., Chiang, C.H., Ponnusamy, K., Ming, G.L., and Song, H. (2008). G9a and Jhdm2a regulate embryonic stem cell fusion-induced reprogramming of adult neural stem cells. Stem Cells *26*, 2131–2141.

Ma, D.K., Jang, M.H., Guo, J.U., Kitabatake, Y., Chang, M.L., Pow-Anpongkul, N., Flavell, R.A., Lu, B., Ming, G.L., and Song, H. (2009). Neuronal activity-induced Gadd45b promotes epigenetic DNA demethylation and adult neurogenesis. Science *323*, 1074–1077.

Mills, E.A., Davis, C.H., Bushong, E.A., Boassa, D., Kim, K.Y., Ellisman, M.H., and Marsh-Armstrong, N. (2015). Astrocytes phagocytose focal dystrophies from shortening myelin segments in the optic nerve of Xenopus laevis at metamorphosis. Proc. Natl. Acad. Sci. USA *112*, 10509–10514.

Ming, G.L., and Song, H. (2011). Adult neurogenesis in the mammalian brain: significant answers and significant questions. Neuron *70*, 687–702.

Mira, H., Andreu, Z., Suh, H., Lie, D.C., Jessberger, S., Consiglio, A., San Emeterio, J., Hortigüela, R., Marqués-Torrejón, M.A., Nakashima, K., et al. (2010). Signaling through BMPR-IA regulates quiescence and long-term activity of neural stem cells in the adult hippocampus. Cell Stem Cell *7*, 78–89.

Muzumdar, M.D., Tasic, B., Miyamichi, K., Li, L., and Luo, L. (2007). A global double-fluorescent Cre reporter mouse. Genesis *45*, 593–605.

Nagata, S., Hanayama, R., and Kawane, K. (2010). Autoimmunity and the clearance of dead cells. Cell *140*, 619–630.

Neher, J.J., Emmrich, J.V., Fricker, M., Mander, P.K., Théry, C., and Brown, G.C. (2013). Phagocytosis executes delayed neuronal death after focal brain ischemia. Proc. Natl. Acad. Sci. USA *110*, E4098–E4107.

Paik, J.H., Ding, Z., Narurkar, R., Ramkissoon, S., Muller, F., Kamoun, W.S., Chae, S.S., Zheng, H., Ying, H., Mahoney, J., et al. (2009). FoxOs cooperatively regulate diverse pathways governing neural stem cell homeostasis. Cell Stem Cell *5*, 540–553.

Pollen, A.A., Nowakowski, T.J., Chen, J., Retallack, H., Sandoval-Espinosa, C., Nicholas, C.R., Shuga, J., Liu, S.J., Oldham, M.C., Diaz, A., et al. (2015).

Molecular identity of human outer radial glia during cortical development. Cell *163*, 55–67.

Porcheri, C., Suter, U., and Jessberger, S. (2014). Dissecting integrin-dependent regulation of neural stem cell proliferation in the adult brain. J. Neurosci. *34*, 5222–5232.

Raymond, A., Ensslin, M.A., and Shur, B.D. (2009). SED1/MFG-E8: a bi-motif protein that orchestrates diverse cellular interactions. J. Cell. Biochem. *106*, 957–966.

Renault, V.M., Rafalski, V.A., Morgan, A.A., Salih, D.A., Brett, J.O., Webb, A.E., Villeda, S.A., Thekkat, P.U., Guillerey, C., Denko, N.C., et al. (2009). FoxO3 regulates neural stem cell homeostasis. Cell Stem Cell *5*, 527–539.

Sato, A., Sunayama, J., Matsuda, K., Tachibana, K., Sakurada, K., Tomiyama, A., Kayama, T., and Kitanaka, C. (2010). Regulation of neural stem/progenitor cell maintenance by PI3K and mTOR. Neurosci. Lett. *470*, 115–120.

Seib, D.R., Corsini, N.S., Ellwanger, K., Plaas, C., Mateos, A., Pitzer, C., Niehrs, C., Celikel, T., and Martin-Villalba, A. (2013). Loss of Dickkopf-1 restores neurogenesis in old age and counteracts cognitive decline. Cell Stem Cell *12*, 204–214.

Shen, Q., Wang, Y., Kokovay, E., Lin, G., Chuang, S.M., Goderie, S.K., Roysam, B., and Temple, S. (2008). Adult SVZ stem cells lie in a vascular niche: a quantitative analysis of niche cell-cell interactions. Cell Stem Cell *3*, 289–300.

Shin, J., Berg, D.A., Zhu, Y., Shin, J.Y., Song, J., Bonaguidi, M.A., Enikolopov, G., Nauen, D.W., Christian, K.M., Ming, G.L., and Song, H. (2015). Single-cell RNA-seq with waterfall reveals molecular cascades underlying adult neurogenesis. Cell Stem Cell *17*, 360–372.

Song, H., Stevens, C.F., and Gage, F.H. (2002). Astroglia induce neurogenesis from adult neural stem cells. Nature *417*, 39–44.

Song, J., Zhong, C., Bonaguidi, M.A., Sun, G.J., Hsu, D., Gu, Y., Meletis, K., Huang, Z.J., Ge, S., Enikolopov, G., et al. (2012). Neuronal circuitry mechanism regulating adult quiescent neural stem-cell fate decision. Nature *489*, 150–154.

Sun, G.J., Zhou, Y., Ito, S., Bonaguidi, M.A., Stein-O'Brien, G., Kawasaki, N.K., Modak, N., Zhu, Y., Ming, G.L., and Song, H. (2015a). Latent tri-lineage potential of adult hippocampal neural stem cells revealed by Nf1 inactivation. Nat. Neurosci. *18*, 1722–1724.

Sun, G.J., Zhou, Y., Stadel, R.P., Moss, J., Yong, J.H., Ito, S., Kawasaki, N.K., Phan, A.T., Oh, J.H., Modak, N., et al. (2015b). Tangential migration of neuronal precursors of glutamatergic neurons in the adult mammalian brain. Proc. Natl. Acad. Sci. USA *112*, 9484–9489.

Yan, L., Yang, M., Guo, H., Yang, L., Wu, J., Li, R., Liu, P., Lian, Y., Zheng, X., Yan, J., et al. (2013). Single-cell RNA-seq profiling of human preimplantation embryos and embryonic stem cells. Nat. Struct. Mol. Biol. *20*, 1131–1139.

Yuzwa, S.A., Borrett, M.J., Innes, B.T., Voronova, A., Ketela, T., Kaplan, D.R., Bader, G.D., and Miller, F.D. (2017). Developmental emergence of adult neural stem cells as revealed by single-cell transcriptional profiling. Cell Rep. *21*, 3970–3986.

Zeisel, A., Muñoz-Manchado, A.B., Codeluppi, S., Lönnerberg, P., La Manno, G., Juréus, A., Marques, S., Munguba, H., He, L., Betsholtz, C., et al. (2015). Brain structure. Cell types in the mouse cortex and hippocampus revealed by single-cell RNA-seq. Science *347*, 1138–1142.

STAR★METHODS

KEY RESOURCES TABLE

REAGENT or RESOURCE	SOURCE	IDENTIFIER
Antibodies		
Cy2-, Cy3-, or Cy5-conjugated donkey secondary	JacksonImmunoResearch	N/A
Cy3-conjugated goat anti-Armenian Hamster secondary	JacksonImmunoResearch	127-165-160; RRID: AB_2338989
Chicken anti-GFP	Aves Labs	GFP-1020; RRID: AB_10000240
Armenian Hamster anti-Mfge8	MBL	D199-3; RRID: AB_590479
Mouse anti-Mfge8	R&D Systems	MAB2767; RRID: AB_2142466
Mouse anti-Mfge8	Santa Cruz	sc-8029; RRID: AB_627950
Mouse anti-GM130	BD Biosciences	610822; RRID: AB_10015242
Rabbit anti-Ki67	Leica	NCL-Ki67p; RRID: AB_442102
Mouse anti-Ki67	BD Biosciences	550609; RRID: AB_393778
Mouse anti-BM28 (aka Mcm2)	BD Biosciences	610701; RRID: AB_398024
Rat anti-BrdU	Novus	NB500-169; RRID: AB_10002608
Goat anti-Nestin	Santa Cruz	sc-21248; RRID: AB_2148925
Chicken anti-Nestin	Aves Labs	NES; RRID: AB_2314882
Mouse anti-GFAP	Millipore	MAB360; RRID: AB_11212597
Rabbit anti-GFAP	DAKO	Z0334; RRID: AB_10013382
Rabbit anti-Tbr2	Abcam	ab23345; RRID: AB_778267
Goat anti-DCX	Santa Cruz	sc-8067; RRID: AB_2088491
Mouse anti-NeuN	Millipore	MAB377; RRID: AB_2298772
Mouse anti-NeuN, Alexa Fluor 488 conjugated	Millipore	MAB377X; RRID: AB_2149209
Rabbit anti-S100β	Sigma	S2644; RRID: AB_477501
Guinea pig anti-Olig2	B. Novitch (University of California, Los Angeles)	N/A
Goat anti-Itga8	R&D Systems	AF4076; RRID: AB_2296280
Sheep anti-Itgb5	R&D Systems	AF3824; RRID: AB_1151977
Rat anti-Itgb1	Millipore	MAB1997; RRID: AB_2128202; (Brooker et al., 2016)
Mouse anti-S6 (54D2)	Cell Signaling	#2317; RRID: AB_2238583; (Kim et al., 2009)
Rabbit anti-pS6 (Ser235/236)	Cell Signaling	#2211; RRID: AB_331679; (Kim et al., 2009)
Rabbit anti-4EBP1 (53H11)	Cell Signaling	#9644; RRID: AB_2097841
Rabbit anti-p4EBP1 (T37/46)	Cell Signaling	#2855; RRID: AB_560835
Mouse anti-Akt (5G3)	Cell Signaling	#2966; RRID: AB_823417
Rabbit anti-pAkt (Thr308)	Cell Signaling	#9275S; RRID: AB_329828
Rat anti-CD68	Bio-Rad	MCA1957GA; RRID: AB_324217
Rabbit anti-Iba1	WAKO	019-19741; RRID: AB_839504
Anti-fluorescein peroxidase	Roche	11426346910; RRID: AB_840257
Hamster anti-rat CD29	BD Biosciences	555002; RRID: AB_395636
Mouse IgG1 isotype control	BD Biosciences	554121; RRID: AB_395252
Rat anti-mouse CD51, integrin αv	BioLegend	104107; RRID: AB_2265155
Mouse anti-β-actin	Sigma	A1978; RRID: AB_476692
Goat anti-rabbit IgG-HRP	Cell Signaling	7074S; RRID: AB_2099233
Goat anti-mouse IgG-HRP	Santa Cruz	sc-2031; RRID: AB_631737
Chemicals, Peptides, and Recombinant Proteins		
DAPI	Thermo Fisher Scientific	D1306; RRID: AB_2629482
Paraformaldehyde	Electron Microscopy Sciences	19210

(Continued on next page)

REAGENT or RESOURCE	SOURCE	IDENTIFIER
Dulbecco's Phosphate-Buffered Saline (DPBS)	Corning	21-031
10x Target Retrieval solution	DAKO	S1699
Donkey serum	Sigma	D9663
Proteinase K	Thermo Fisher Scientific	AM2548
Tamoxifen	Sigma	T5648
Corn oil	Sigma	C8267
BrdU	Sigma	B9285
Boric acid	Sigma	B0252
Rapamycin	LC Laboratories	R-5000
Tween-80	Sigma	P1754
PEG 400	Sigma	1546445
EdU	Thermo Fisher Scientific	A10044
Matrigel matrix	Corning	354277
Phosphatase inhibitor cocktail	Cell Signaling	5870
Protease inhibitor cocktail	Sigma	P8340
4-Hydroxy-tamoxifen	Sigma	H6278
Dulbecco's Modification of Eagle's Medium (DMEM)	Corning	10-013
Neurobasal Medium	GIBCO	21103049
GlutaMAX Supplement	GIBCO	35050061
Penicillin-Streptomycin (10,000 U/mL)	GIBCO	15140122
B-27 Supplement	GIBCO	17504044
Recombinant Human EGF Protein	BioLegend	585508
Recombinant Human FGF-basic	Peprotech	100-18B
Recombinant Mouse MFG-E8	R&D systems	2805-MF-050
Critical Commercial Assays		
Fast SYBR Green Master Mix	Thermo Fisher Scientific	4385610
Tyramide Signal Amplification Plus Cy3 system	Perkin-Elmer	NEL744
Click-iT Plus EdU Alexa Fluor 647 Imaging Kit	Invitrogen	C10640
Amicon Ultra-4 Centrifugal Filter Units, 10,000 NMWL	Millipore	UFC801008
Experimental Models: Cell Lines		
Adult mouse hippocampal neural stem cells	N/A	N/A
Experimental Models: Organisms/Strains		
Mouse: Adult C57Bl6/J	Charles River	N/A
Mouse: *Mfge8*$^{-/-}$ (germline knockout)	(Hanayama et al., 2004)	IMSR Cat# RBRC01726, RRID: IMSR_RBRC01726
Mouse: *Mfge8*$^{f/f}$ (conditional knockout)	Atabai lab, unpublished	N/A
Mouse: Nestin-GFP	(Encinas et al., 2006)	N/A
Mouse: *Gli1-CreER*^{T2}	(Ahn and Joyner, 2005)	MGI Cat# 4838613, RRID: MGI:4838613
Mouse: *mT/mG* $^{f/f}$	(Muzumdar et al., 2007)	N/A
Software and Algorithms		
Imaris 7.2, 7.6, and 9.0	Bit Plane	http://www.bitplane.com/imaris/imaris
ImageJ	NIH	RRID: SCR_003070; https://imagej.nih.gov/ij/
Origin 6.0 and 8.0	OriginLab	https://www.originlab.com/
Other		
PCR primers for genotyping	See Table S1	N/A
Mini-PROTEAN TGX Precast Protein Gels	Bio-Rad	4561033
Trans-Blot Turbo Mini PVDF Transfer Packs	Bio-Rad	1704156
Trans-Blot Turbo Transfer Starter System	Bio-Rad	1704155
Confocal Microscope	Zeiss	710 and 800
Frozen Sliding Microtome	Leica	SM2010R

CONTACT FOR REAGENT AND RESOURCE SHARING

Further information and requests for resources and reagents should be directed to and will be fulfilled by the Lead Contact, Hongjun Song (shongjun@pennmedicine.upenn.edu). There are no restrictions on any data or materials presented in this paper.

EXPERIMENTAL MODEL AND SUBJECT DETAILS

Animals

All animal procedures used in this study were performed in accordance with the protocol approved by the Institutional Animal Care and Use Committee of Johns Hopkins University School of Medicine and University of Pennsylvania. All mice in the study were back-crossed to the C57BL/6 background for at least six generations. Animals were housed in a 14-hour light/10-hour dark cycle and had free access to food and water. Housing and husbandry conditions followed standard settings. Both 15-day-old mice (postnatal) and 2-month-old mice (adult) were used in this study. For immunohistology, C57Bl6/J wild-type mice and *Nestin-GFP* transgenic mice (Encinas et al., 2006) were used. For knockout and rapamycin rescue analysis, mice used in different groups were housed as litter-mates: C57Bl6/J WT mice, and *Mfge8$^{-/-}$*(KO). For conditional knockout analyses, *Gli-CreER^{T2}; Mfge8$^{f/f}$*; *mT/mG$^{f/-}$*, and *Gli1-CreER^{T2}; mT/mG$^{f/-}$* were generated by crossing *Gli1-CreER^{T2}* driver (Ahn and Joyner, 2005) with *mT/mG$^{f/-}$* reporter (Muzumdar et al., 2007) and *Mfge8$^{f/f}$* mice (Atabai lab), where applicable. Primers used for mouse genotyping were listed in Table S1.

METHOD DETAILS

BrdU administration

For analysis of cell proliferation in the dentate gyrus, P15 or P60 mice were injected with BrdU (200 mg/kg body weight, i.p.) and analyzed 2 hours or 30 days later. Tissue processing and quantification of BrdU$^+$ cells within the SGZ and granule cell layer were carried out as previously described (Jang et al., 2013).

Tamoxifen administration

Tamoxifen (66.67 mg/ml, Sigma, T5648) was prepared in a 5:1 corn oil (Sigma) to ethanol mixture (Sun et al., 2015a; Sun et al., 2015b). A dose of 375 mg/kg body weight was intraperitoneally injected into P15 or P60 male and female mice every 12 hours for 3 times. Mice were analyzed 3 or 30 days post-tamoxifen injection.

Rapamycin administration

Rapamycin (LC Laboratories) was first dissolved in ethanol at a stock concentration of 25 mg/ml and was further diluted with a final concentration of 1 mg/ml in 4% ethanol, 5% Tween 80, and 5% PEG 400 as previously described (Kim et al., 2009). Rapamycin was intraperitoneally delivered twice to mice at 20 mg/kg body weight at P11 and P13, analyzed at P15, or injected at P60 and P62 and analyzed at P64.

Tissue processing, immunostaining, and confocal imaging

Animals were perfused with cold 4% paraformaldehyde [wt/vol; in 0.1 M phosphate buffer (PB), pH 7.4], and cryoprotected with 30% sucrose (wt/vol). Serial 40-μm-thick coronal brain sections were cut on a frozen sliding microtome (Leica; SM2010R) for immunohis-tology as previously described (Sun et al., 2015a; Sun et al., 2015b). Every 6th section was taken for immunohistology throughout the anterior to posterior axis of the dentate gyrus. Antibodies were diluted in TBS (Tris buffered saline) with 0.1% Triton X-100 and 3% (vol/vol) donkey serum. Sections were incubated with primary antibodies at 4°C overnight. The following primary antibodies were used: BrdU (Novus; rat; 1:300), CD68 (Bio-Rad; rat; 1:300), DCX (Santa Cruz, goat, 1:100), GFAP (Millipore, mouse, rabbit, 1:1,000), GFP (Aves Labs, chicken, 1:500), GM130 (BD Biosciences, mouse, 1:300), Iba1 (WAKO; rabbit; 1:500), integrin α$_8$ (R&D Systems; goat; 1:100), integrin β$_1$ (Millipore; rat; 1:300), integrin β$_5$ (R&D Systems; sheep; 1:500), Ki67 (Leica; rabbit; 1:500; BD Bioscience; mouse; 1:500), Mcm2 (aka BM28; BD Biosciences; mouse; 1:300), Mfge8 (MBL; Armenian Hamster; 1:500; R&D Systems; Mouse; 1:100; Santa Cruz; mouse; 1:300), Nestin (Santa Cruz; Goat; 1:250; Aves Labs; chicken; 1:500), NeuN (Millipore; mouse; 1:500; and Alexa Fluor 488 conjugated), Oligo2 (guinea pig; 1:500); p4EBP1 (Cell Signaling; rabbit; 1:500), pS6 (Ser-235/236; Cell Signaling; rabbit; 1:500), S-100β (Sigma; rabbit; 1:300); and Tbr2 (Abcam; rabbit; 1:250).

The mT-labeled cells and non-specific blood vessel labeling were removed, and Mcm2 and NeuN antigens were retrieved by incu-bating brain sections in 1 X target retrieval solution (DAKO) at 92.5°C for 10 min, followed by a 20-min cooling to room temperature. BrdU antigen was retrieved by incubating brain sections in 2N HCl for 1 hour in room temperature, followed by 0.1M boric acid neutralization for 30 min. Cy2-, Cy3- or Cy5-conjugated secondary antibodies (Jackson ImmunoResearch; 1:500) to appropriate species were incubated at room temperature for 2 hours. Stained sections were imaged at 40x on a Zeiss LSM 710 or 800 confocal microscope (Carl Zeiss).

In situ hybridization

In situ hybridization was performed on PFA-fixed brain sections (40 μm thickness) as described previously (Ma et al., 2009; Mills et al., 2015). Fluorescein-conjugated antisense riboprobe for *Mfge8* mRNA was generated by *in vitro* transcription. Hybridization of the

riboprobes on sections was performed at 65°C overnight and followed by washing once with 5x SSC and 1% SDS, then twice with 0.2x SSC for 1 hour each at 72°C. The sections were incubated with anti-fluorescein peroxidase (Roche) at 4°C overnight, and were visualized using Cy3-conjugated Tyramide Signal Amplification system (Perkin-Elmer) at room temperature. The *in situ* hybridization was followed by immunostaining for Nestin (goat anti-Nestin, Santa Cruz, 1:500), and GFAP (Millipore, mouse, rabbit, 1:1,000) incubated at 4°C overnight and followed by incubation of Cy2- and Cy5-conjugated secondary antibodies (Jackson ImmunoResearch; 1:500) for 2 hours at room temperature.

Adult neural progenitor culture and analyses

Adult mouse hippocampal neural progenitor cells were derived from adult mouse dentate gyrus as previously described (Ma et al., 2008; Song et al., 2002). To determine whether Mfge8 was secreted by adult neural progenitors in culture, cells were cultured to reach 75% confluency and media were collected and concentrated 5-10 times by centrifugation at 4°C with Amicon Ultra-4 Centrifugal Filter Units (Millipore, 10,000 NMWL) at 4,000 x g. Samples were processed for western blot analysis to detect Mfge8 protein at ∼50 KD.

To examine neural progenitor proliferation, adult neural progenitors were incubated with exogenous recombinant Mfge8 (R&D Systems) for 2 days. Blocking antibodies against integrin α_v (BioLegend; 0.625 μg/ml) or β_1 (BD Biosciences; 0.625 μg/ml), or IgG control (BD Biosciences; 0.625 μg/ml) were added for 24 hours before an EdU (Thermo Fisher Scientific, 10 μM) pulse for 40 min followed by PFA fixation for immunostaining, imaging and quantification. EdU was detected by Click-iT Imaging Kit (Invitrogen), in combination with immunostaining for Nestin (goat anti-Nestin, Santa Cruz, 1:500).

Biochemical analyses were performed as previously described (Kim et al., 2009). Adult neural progenitor culture was lysed in cold RIPA buffer containing 50 mM Tris HCl (pH 7.5), 150 mM NaCl, 1% NP-40, 0.5% sodium deoxycholate, 0.1% SDS supplemented with protease and phosphatase inhibitor cocktail (Cell Signaling; Sigma) at 4°C for 10 min, followed by sonication on ice for 30 s for 3 times. Protein concentration was determined by Bradford assay (Bio-Rad). Equal amounts of protein were loaded to be separated by SDS-PAGE on 4%–20% resolving gels (Bio-Rad) and transblotted onto PVDF membranes (Bio-Rad). Membranes were incubated in primary antibodies at a 1:1,000 dilution at 4°C overnight against 4EBP1 (Cell Signaling; rabbit), p4EBP1 (Cell Signaling; rabbit), S6 (Cell Signaling; mouse), pS6 (Cell Signaling; rabbit), β-actin (Sigma; mouse), Mfge8 (R&D Systems; mouse; Santa Cruz; mouse), Akt (Cell Signaling; mouse), and pAkt (Cell Signaling; rabbit), followed by a secondary HRP-conjugated antibody (Cell Signaling; rabbit; Santa Cruz; mouse). For evaluation of total 4EBP1, S6, and Akt, we stripped and reprobed membranes that had been blotted for phospho-versions of these proteins.

Image processing and data analyses

All confocal images were blindly acquired between experimental and control groups under the same laser power and gain, and were analyzed with Imaris 7.2, 7.6, 9.0 software (BitPlane), or ImageJ (NIH) without adjusting image brightness or contrast, as previously described (Sun et al., 2015a; Sun et al., 2015b). The Spots module in Imaris was used to digitize cell-nucleus locations in the 3D space and to code cell type classifications according to distinct morphological and molecular markers. The Clipping Plane module in Imaris was used to estimate the local SGZ plane for 2D clone projections. For illustrative purposes, some cells and features were volume-rendered using the Surface module in Imaris (Figures 1C–1F; bottom panels). A confirmed RGL needed to satisfy the following criteria, (1) located in the SGZ of the dentate gyrus; (2) have a distinct Nestin$^+$GFAP$^+$ radial process; and (3) have a DAPI$^+$ nuclei that is largely wrapped around by GFAP immunostaining signal in the same focal plane (Bonaguidi et al., 2011; Song et al., 2012). A cell nucleus located within the granule cell layer and having overlapped immunostaining signals of DAPI, BrdU/Mcm2, and Tbr2 or NeuN in the same focal plane, was defined as a BrdU$^+$/Mcm2$^+$ intermediate progenitor cell or dentate granule neuron, respectively. A BrdU$^+$/Mcm2$^+$ DCX$^+$ neuroblast should be located in the granule cell layer and have a DAPI$^+$ and BrdU$^+$/Mcm2$^+$ nuclei that is largely wrapped around by DCX immunostaining signal in the same focal plane.

QUANTIFICATION AND STATISTICAL ANALYSIS

The studies were blinded during data collection and quantification. Data in figure panels reflect several independent experiments performed on different days. No data were excluded. An estimate of variation within each group of data is indicated using standard error of the mean (SEM). Statistical analysis was performed with one-way ANOVA (with Tukey post hoc test), or one-tailed unpaired Student's t test, as indicated in the text and figures. All statistical analyses were performed in Origin software (OriginLab).